

ASSESSMENT OF OVER-CURRENT PROTECTION FOR SUPERCONDUCTING CABLES

Eleni Tsotsopoulou^{1}, Adam Dysko¹, Dimitrios Tzelepis¹*

¹*Department of Electronic and Electrical Engineering, University of Strathclyde, Glasgow, United Kingdom*

**eleni.tsotsopoulou.2018@uni.strath.ac.uk*

Keywords: SUPERCONDUCTING CABLE, OVERCURRENT PROTECTION, QUENCHING

Abstract

The objectives of the studies presented in this paper aim to assess the sensitivity and the stability margins of conventional over-current protection schemes for the protection of Superconducting Cables with High Temperature Superconducting tapes. The ultimate goal is to identify the limitations and particularities of the conventional over-current relays to provide sensitive and reliable protection for the superconducting-based power grids. For this purpose, a verified model of Superconducting Cable developed in Matlab/Simulink and has been utilized to examine its transient performance and obtain profound insights of the quenching phenomenon. The case studies include different types of internal faults applied on the Superconducting Cable and external faults occurring on the adjacent feeders. The results and observations included in the paper, identified that due to the inherent dynamically changing resistance and the mutable operating stages of the SC, the reliability and the discriminative capability of the conventional over-current relays are compromised.

1 Introduction

In recent years, the deployment of multi-layer Superconducting Cable (SC) systems, with second generation (2G) High Temperature Superconducting (HTS) wires, have been gradually entered the stage of engineering applications to respond to the changing characteristics of modern power grids. Conversely to the conventional copper cables, SCs are characterized by a plethora of technically-attractive attributes such as higher current-carrying capability, higher power transfer at lower operating voltages and over longer distances, minimization of power losses [1], compact size [2], etc. With this trend, the SC applications are being actively studied around the world. Furthermore, an increasing attention has been given to the SCs with inherent fault current limiting capability; i.e. like the ConEd project in Chicago [3]. In more specific, these type of SCs, satisfy both the large capacity power transmission and the limitation of the fault currents, which is an advantageous feature for the densely populated areas which are characterized by increasing electrical power installation. Nevertheless, the inclusion of SCs with fault current limiting capability, gives a rise to many fault-related challenges accounting for the sensitivity and stability of conventional protection schemes as well as the protection coordination, emanating from the quenching phenomenon in line with the dynamically-changing impedance.

The performance of the SCs is predominantly dependent on the unique electromagnetic features of the HTS tapes, which form the basis of the manufacture of the HTS cable, and the cable geometry (i.e. cable diameter, pitch angle, gap between layers). During steady state conditions, HTS tapes operate in superconducting state, presenting approximately zero resistance. However, in transient conditions (i.e. faults) when the current flowing through the HTS tapes increases significantly, HTS tapes start to lose their superconducting

properties, due to the quenching phenomenon. The three parameters that determine the quenching process are the critical current I_C , the critical temperature T_C and the critical magnetic field H_C . The quenching process initiates once the fault current exceeds the value of the critical current I_C . As the fault current continues to increase, the resistivity of the HTS rises exponentially, leading to the rise in temperature and subsequently to generation of joule heat. When temperature becomes higher than the critical temperature T_C , HTS tapes lose completely their superconducting features and enter the highly resistive state. The current is then diverted to the parallel-connected copper stabilizer layer, and the copper former which both operate as an alternative path for the fault current. Hence, the transition of the HTS tapes to the highly resistive state enforces the appearance of resistance which imposes i) the current redistribution, ii) a dynamic change in the equivalent impedance of the system, and iii) the reduction of the fault current to a certain value. The decreased fault current depends not only on the system's condition but on the characteristics of the SC. The variable system's impedance has a negative impact on the well-establish protection schemes (i.e distance and over-current relays) and it adversely affects the protection coordination. Additionally, one major challenge of the fault detection on SCs has been reported in [4]. It was revealed that during highly resistive faults, the fault current is predominantly reduced by the fault resistance, affecting the quenching process, and making the fault identification an even more challenging task.

Many researchers have studied the impact of the quenching on the conventional protection schemes. In [5], a review of the protection problems which can be caused by a 154kV smart SC in South Korea system is presented. The work in [6] proposes a decision-making algorithm to improve the performance of the conventional differential and overcurrent relays. The presented work analyzes the quenching mechanism

under different transient events and aims to assess the sensitivity and stability margins of the conventional overcurrent relays and identify their limitations to provide discriminative protection for the SC-based grids. For this purpose, a model of SC has been developed in Matlab/Simulink software and a verified IDMT have been utilized.

2 Methodology

2.1 SC Modelling.

A verified SC model developed in [4] with 2G HTS conductor coated in Yttrium Barium Copper Oxide (YBCO) material, has been utilized in order to investigate its electro-thermal behavior and the subsequent impact on the over-current protection. The cable core consists of several layers of HTS tapes, which are helically wound on a copper former. Figure 1 shows a simplified structure diagram of the HTS tape.

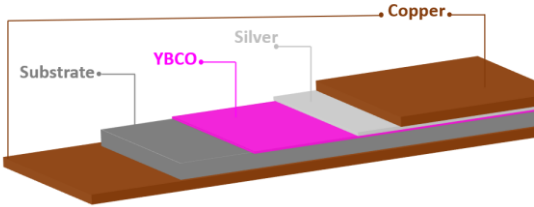


Figure 1: Cross section of the HTS tape.

The employed tapes composed of one YBCO layer, two copper stabilizer layers, substrate and silver layers [7]. Polypropylene laminated paper (PPLP) was applied on the HTS tapes and was utilized as electric insulation, while a cryostat with liquid nitrogen LN_2 was utilized as refrigerant for cooling the SC at 70K. The structure of the cable is 3-in-One, considering the three phases contained in one cryostat, offering the advantage of reduced installation space and heat invasion compared to other cable configurations. Table 1 lists the physical parameters and the specifications of the developed SC model.

Table 1: Parameters of SC cable.

Parameters	Values
Number of tapes N_t	15
Tape width	4 mm
YBCO layer thickness	1 μm
Copper layer thickness	40 μm
Substrate layer thickness	60 μm
Silver layer thickness	3.8 μm
Critical temperature T_C	92 K
Operating temperature	70 K
Tape critical current at 70 K I_C	250 A
Cable length	5 km
Operating voltage	33 kV

The calculation process of the electro-thermal modelling is presented in Figure 2. The values of the critical current I_C , the critical temperature T_C and the working magnetic field B , are the main factors that affect the quenching process and

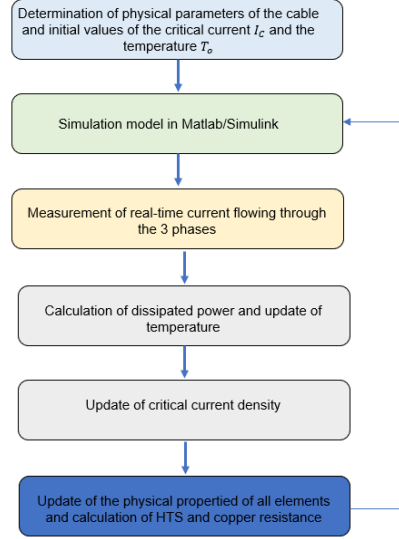


Figure 2: Flowchart of the simulation routine.

consequently the resistivity of the HTS tapes. The critical current density J_C of HTS tapes can be expressed as a function of the temperature as described in (1),

$$J_C(T) = \begin{cases} J_{C,in}(B) \cdot \frac{(T_C - T(t))^a}{(T_C - T_o)^a}, & T < T_C \\ 0, & T > T_C \end{cases} \quad (1)$$

where $J_{C,in}$ is the initial critical current density (A/m^2) at initial temperature $T_o = 70 K$ and at working magnetic field B , T_C is the critical temperature (K) and a denotes the density exponent which is conventionally set to 1.5 for the YBCO material [8]. Based on (1), during the quenching process, as the temperature $T(t)$ increases, the value of the critical current density J_C decreases accordingly. When the temperature exceeds critical temperature T_C , the current density is reduced to 0.

In order to develop a suitable model for the SC, the $E - J$ power law must be considered, which expresses the non-linear relationship between the voltage and current of the HTS tape and is used to derive the resistivity of the superconductor based on (2) [9],

$$\rho_{SC} = \frac{E_C}{J_C(T)} \cdot \left(\frac{J}{J_C(T)} \right)^{N-1} \quad (2)$$

where E_C is the critical electric field equal to 1 $\mu\text{V}/\text{cm}$ and the coefficient N has been set to 30 according to [8]. During the superconducting state, the resistivity of the HTS tapes is $\rho_{SC} = 0$ and the superconductor behaves as an ideal conductor. When the applied current exceeds the critical value I_C , the resistivity of the HTS tapes arises sharply and it results in the appearance of a resistance. At this stage, the HTS tapes have entered the flux flow state and the current tends to start flowing through the copper stabilizer layers and the copper former. The exponential increase in the resistivity causes the generation of joule heating, leading to an increase in the temperature of the superconductor. Once the temperature surpasses the critical temperature T_C , the HTS tapes enter the highly resistive state,

presenting high values of resistance and the fault current is fully diverted to the copper stabilizer and former layers which have lower resistivity.

The resistivity of the copper ρ_{Cu} is then given as a function of the temperature by (3) [9],

$$\rho_{Cu} = (0.0084 \cdot T - 0.4603) \cdot 10^{(-9)}, 250 K > T > 70K \quad (3)$$

Based on the above analysis, it can be concluded that the equivalent resistance of the superconductor is varied depending on the operating state of the HTS tapes due to the quench phenomenon. In more specific, R_{eq} of the superconductor is calculated as the equivalent resistance of parallel electrical circuits considering the current distribution between the YBCO layers, the copper stabilizer layers and the copper former. The obtained expressions with respect to the current and the temperature can be given by (4),

$$R_{eq} = R_{SC} // R_{Copper} = \begin{cases} R_{SC}, & T < T_C, I < I_C \\ R_{SC} // R_{Copper}, & T < T_C, I > I_C \\ R_{Copper}, & T > T_C, I > I_C \end{cases} \quad (4)$$

The increase in the temperature can be obtained based on (5),

$$T(t) = T_o + \frac{1}{C_p} \cdot \int_0^t P_{SC}(t) dt \quad (5)$$

where C_p (J/K) denotes the heat capacity of each material and is calculated by the multiplication of the specific heat by the volume and the density of each material. P_{SC} is the net power in the superconductor and is given by the thermal equilibrium equation (6),

$$P_{SC}(t) = P_{diss}(t) - P_{cooling}(t) \quad (6)$$

where $P_{diss}(t)$ is the generated joule heating in superconductor given by (7) and $P_{cooling}(t)$ is the power dissipated by the refrigerant LN_2 , given by (8).

$$P_{diss}(t) = I^2(t) \cdot R_{eq}(t) \quad (7)$$

$$P_{cooling}(t) = h \cdot A \cdot (T(t) - 70) \quad (8)$$

where A is the surface area covered by the LN_2 and h is the heat transfer coefficient which is temperature-dependent and considered the main factor which determines the effectiveness of the cooling system to remove the dissipated heat from the superconductor. For the calculation process an empirical formula has been utilized for the h according to [10].

Equations (2) to (8) represent a multi-physics bi-directional coupling, as the applied current is translated into generated joule heating and the temperature variations result in changes of the material resistivity. For the electro-thermal modelling the heat exchange with the external environment has been neglected. Therefore, the total heat generated by the superconductor is absorbed by superconductor itself, leading

to the increase in temperature and the LN_2 by convective heat transfer.

2.1 Power System Model

The studies conducted in this research aim to evaluate the performance of the developed SC under different faults and assess the response of the over-current protection. For the purpose of carrying out transient simulation analysis, a power system model has been developed in Matlab/Simulink software as illustrated in Figure 3 and is utilized for Electromagnetic Transient (EMT) type simulation studies.

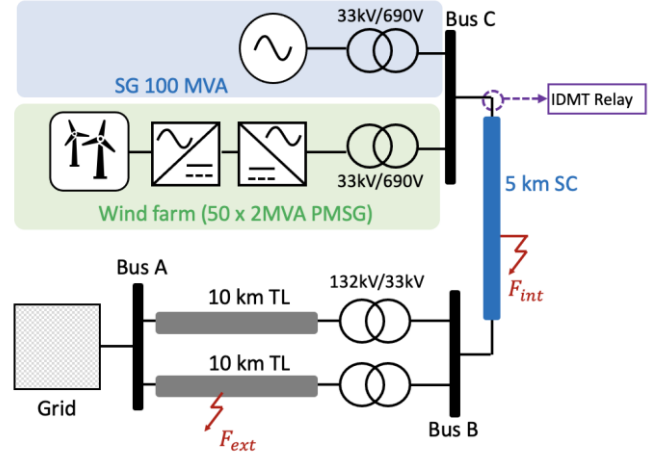


Figure 3: Examined power system.

The network under-test is formed by the equivalent grid (represented by a voltage source) with nominal voltage of 132 kV, and two generating units connected at Bus C, considering a Synchronous Generator (SG) and a wind farm connected via a Voltage Source Converter (VSC). The SG has been modelled as a standard salient-pole synchronous machine rated at 100 MVA with three integrated control systems: i) automatic voltage regulator, ii) power system stabilizer, and iii) over excitation limiter [11] [12]. The wind farm consists of 50 variable speed wind turbines rated at 2 MVA each. The SC has been installed between Bus B and C due to its high-power transfer capability to export to total power provided by the generation units to the wider transmission network.

2.2 Transient performance of SC

A systematic iterative simulation analysis was carried out, using the system depicted in Figure 3. The ultimate goal of the simulation-based studies is to investigate the performance of the SC under different faults considering the dynamic changes and consequently define the protection challenges introduced by the integration of SCs in the grid.

The test cases include internal (F_{int}) and external faults (F_{ext}). All possible types of faults have been considered, accounting for three-phase (LLL), three-phase to ground (LLL-G), phase-to-phase (LL), phase-to-phase to ground (LL-G) and phase-to-ground (L-G) faults with fault resistances up to 50 Ω . The internal faults have been simulated at every 5% of the SC's length, while the external faults have been considered at the adjacent feeders at 132 kV. For all the scenarios an automatic

search routine has been developed to iteratively change the fault location along the SC, the fault resistance and the fault type. During the simulation process time domain signatures of the i) fault currents, ii) resistance and ii) temperature were captured at a sampling frequency of 20 kHz.

Figure 4 shows the fault current signatures of the SC during an LLL-G solid fault at 10% of SC's length, while Figure 5 presents the resulting equivalent resistance and temperature of the SC.

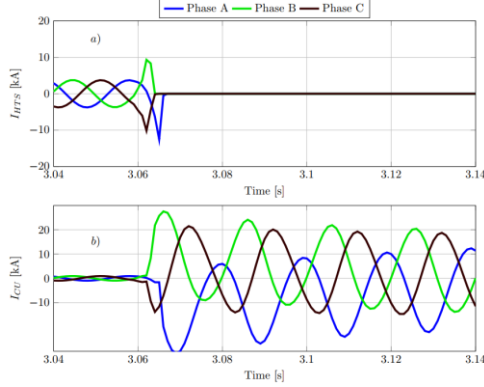


Figure 4: Fault current signatures of SC for a LLL-G solid fault at 10% of the SC's length: (a) currents of HTS layer (b) currents of copper.

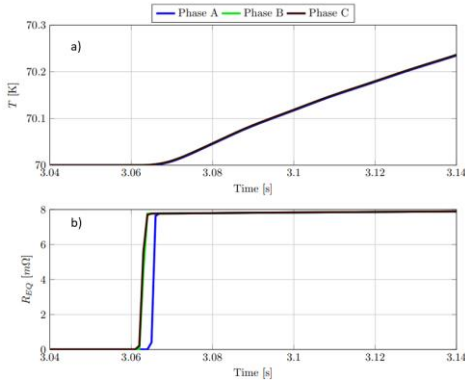


Figure 5: (a) Temperature of SC (b) equivalent resistance of SC for a LLL-G solid fault at 10% of SC's length.

During the steady state condition, the current flows only through the HTS layers for all the phases (Figure 4a). The fault occurs at $t = 3.06$ s and once the fault current exceeds the critical current I_C , the HTS tapes start to quench, resulting in a sharp increase in the resistance and temperature, as depicted in Figure 5a and Figure 5b respectively.

Additionally, the quenching process leads to the fault current redistribution. Specifically, once the resistance of the HTS tapes reaches high value at $t = 3.064$ s, the majority of the fault current is diverted to the copper stabilizer layers and the copper former (Figure 4b). As the quenching phenomenon evolves, the resistivity of the copper increases as a function of the temperature based on (3), leading to the reduction of the fault current. It is noticeable from Figure 4a, that the first peaks of the fault current are 30 kA for phase A, 27.7 kA for phase B and 21.4 kA for phase C, respectively. Due the increase of

the equivalent resistance of the SC, 4 ms after the fault occurrence, the fault current is sustained at approximately 21 kA for phase A, 20 kA for phase B and 14 kA for phase C respectively.

Figure 6 and Figure 7 provide a better insight of the influence of the fault resistance on the quenching process and the subsequent impact on the transient performance of the SC. The fault current signatures illustrated in Figure 6 correspond to a LLL-G fault at 10% of SC's length with fault resistance $R_f = 50 \Omega$.

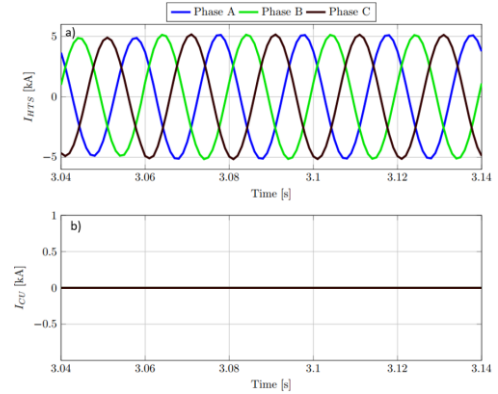


Figure 6: Fault current signatures of SC for a LLL-G fault at 10% of SC's length with $R_f=50 \Omega$: (a) currents of HTS layer (b) currents of copper.

As can be seen in Figure 6a, once the fault occurs at $t = 3.06$ s, the resulting fault current flowing through the HTS tapes does not exceed the value of the critical current I_C and therefore the HTS tapes do not quench. Essentially, there is no current sharing between the HTS layer, the copper stabilizing layers and the copper former, while the equivalent resistance and the temperature remain at 0Ω and 77K which only indicates that the SC operates at superconducting state (Figure 7).

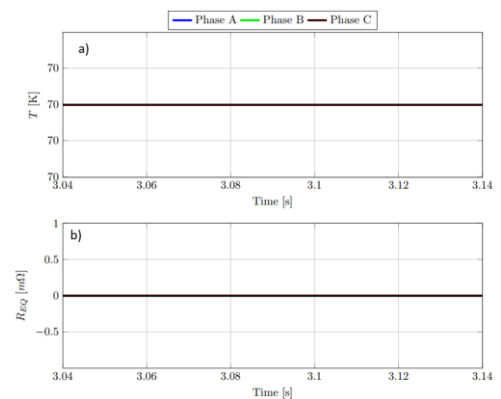


Figure 7: (a) Temperature of SC (b) equivalent resistance of SC for a LLL-G fault at 10% of SC's length with $R_f=50 \Omega$.

This emanates from the fact that the perspective fault current is the main factor which leads the HTS tapes to the quenching. The presence of the high values of fault resistance eliminates the prospective current, preventing the SC from quenching and making the fault detection a more challenging task.

The performance of the SC under other transient events, such as external faults, has been also examined in this work. Figure 8 and Figure 9 depict the resulting behaviour of the SC for a LL-G solid fault at the adjacent 132 kV feeder. As opposed to the highly resistive internal fault, the solid external fault forces the SC to quench. In particular, at $t = 3.06$ s the fault current flowing through the HTS layers reaches peaks equal to 8.45 kA for phase A and 9.88 kA for phase B, respectively. The value of the critical current is exceeded, and the fault current has been diverted to the copper. Therefore, it is observed that other transient events (i.e., external faults at this case) initiate the quenching of the SC, increasing the difficulty in protection discrimination.

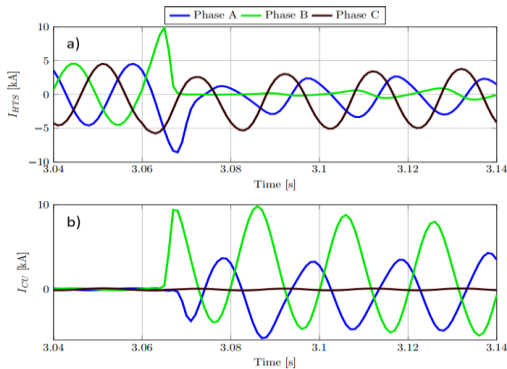


Figure 8: Fault current signatures of SC for a LL-G solid external fault: (a) currents of HTS layer (b) currents of copper.

The performance of the SC under transient events revealed the following significant observations:

- The transition of the SC to the resistive state during the quenching composes a dynamic change to the equivalent impedance of the system and affects the fault current magnitudes and may have adverse impact on the protection schemes such as over-current relays.
- High values of fault resistance predominantly affect the quenching process and make the fault detection challenging.
- External faults initiate the quench of the SC and subsequently it introduces challenges regarding the protection stability and protection coordination

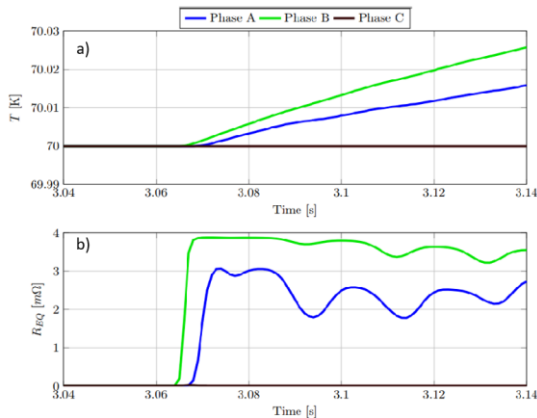


Figure 9: (a) Temperature of SC (b) equivalent resistance of SC for a LL-G soli external fault.

3 Over-current protection performance

This section quantifies the impact of the variable resistance and the quenching process to well-established over-current protection schemes. Specifically, the performance of an over-current relay has been investigated regarding its sensitivity to operate for internal faults and its stability against external faults.

At this regard, a dynamic model of conventional overcurrent relay has been developed in Matlab/Simulink and the fault current signatures obtained from the simulation-based analysis discussed in Section 2 have been imported to the relay for post processing. For the pick-up current setting of the modelled relay a wide range of over-current thresholds has been investigated, starting from 1.05 p.u. to 2 p.u. with step of 0.01 p.u. (base value is the nominal current). Regarding the time settings, different values of time delay has been investigated accounting for 50 ms, 100 ms, 110 ms and 120 ms.

Figure 10 Error! Reference source not found. presents the total number of relay trips for the internal and external fault respectively, with respect to the pick-up current setting. The percentage of the relay trips has been calculated by dividing the total number of the scenarios during which the relay operates, by the total number of the investigated fault scenarios for each case respectively. Based on Figure 10a, it is evident that for lower over-current threshold (1.05 p.u.), 68% of the internal fault have been detected.

Although, as the value of the over-current threshold increases the sensitivity of the over-current relay is jeopardized. Furthermore, as it is indicated in Figure 10b, for lower over-current thresholds (1.05 p.u. to 1.3 p.u.), the stability of the relay is reduced as a trip signal is initiated for the external faults as well, reaching values up to 45%. To improve the stability margins, higher values of over-current thresholds are required, compromising the protection sensitivity.

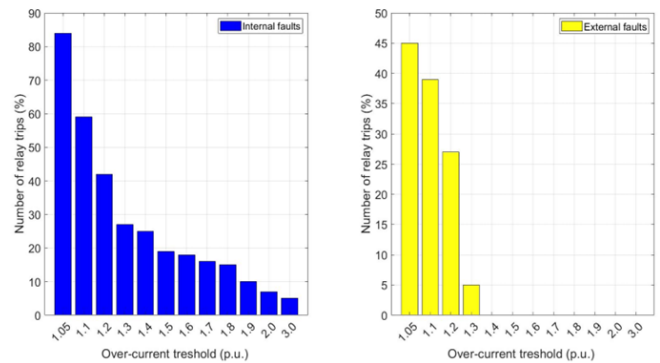


Figure 10: Number of relay trips with respect of the over-current threshold during (a) internal faults (b) external faults.

Additionally, the operation of over-current relay for external faults decreases the protection discrimination capability. Consequently, the presence of the quenching phenomenon during external faults, imposes significant limitations to the

coordination of the protective devices, as the over-current relay may operate faster than the relays on the adjacent lines. Figure 11 presents the number of relay trips with respect to the increase the time delay settings. The over-current threshold has been set equal to $1.05 p.u.$. The results indicate that as the time delay increases, the relay sensitivity is deteriorated and the stability is improved. Specifically, for time delay equal to $120 ms$, the relay remains stable against all the external faults (Figure 11b) but the internal faults remain undetected (Figure 11a). Therefore, the results indicate that conventional protection schemes (i.e., over-current relays) cannot provide reliable protection for SCs, combining both sensitivity and stability.

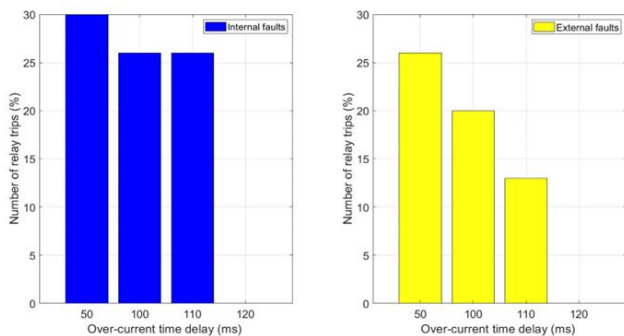


Figure 11: Number of relay trips with respect of time delay settings during (a) internal faults (b) external faults.

4 Conclusions

This paper investigates the sensitivity and stability margins of conventional over-current protection, for protecting SCs against internal and external faults occurring. A verified model of SC with copper stabilizer layers has been integrated within a system which incorporates conventional and inverter-based generating units. The observations obtained from the analysis of the SC's transient performance highlighted that the protection of the SCs is a complex problem due to the quenching phenomenon. In particular, the dynamically changing resistance and the reduced fault currents make the detection of faults a quite challenging problem. The integration of SCs with inherent fault current limiting capability, alongside inverter-based sources, (which are notably characterized by low short-circuit levels), imposes an additional negative impact on the reliability of the conventional protection schemes which operate based on the measurement of the fault current magnitude. At the same time, the presence of external faults may initiate the quenching of SCs, which compromise the discrimination and stability margins of protection. Therefore, the utilization of conventional over-current for SCs' protection is a trade-off between the protection sensitivity and stability.

This work offers a solid foundation for further research on the fault analysis and protection schemes for SCs, which shall consider the unique transient characteristics of the SCs in order to address the identified challenges. The utilization of adaptive protection, the advancements in artificial intelligence-based algorithms for fault detection, and the developments is

distributed sensing technology, are some of the approaches which are worth being investigated for the protection of future power grids incorporating SCs.

References

- [1] J. Zhu, Z. Zhang, H. Zhang, M. Zhang, M. Qiu, and W. Yuan, "Electric measurement of the critical current, AC loss, and current distribution of a prototype HTS cable," *IEEE Trans. Appl. Supercond.*, vol. 24, no. 3, pp. 26–29, 2014, doi: 10.1109/TASC.2013.2284295.
- [2] A. Ballarino *et al.*, "The BEST PATHS Project on MgB₂ Superconducting Cables for Very High Power Transmission," *IEEE Trans. Appl. Supercond.*, vol. 26, no. 3, 2016, doi: 10.1109/TASC.2016.2545116.
- [3] J. Maguire *et al.*, "Status and progress of a fault current limiting HTS cable to be installed in the con Edison grid," *AIP Conf. Proc.*, vol. 1218, no. 3, pp. 445–452, 2010, doi: 10.1063/1.3422388.
- [4] E. Tsotsopoulou *et al.*, "Modelling and fault current characterization of superconducting cable with high temperature superconducting windings and copper stabilizer layer," *Energies*, vol. 13, no. 24, 2020, doi: 10.3390/en13246646.
- [5] E. Y. Ko, S. R. Lee, S. Seo, and J. Cho, "Impact of Smart HTS transmission cable to protection systems of the power grid in South Korea," *IEEE Trans. Appl. Supercond.*, vol. 29, no. 5, pp. 1–5, 2019, doi: 10.1109/TASC.2019.2908611.
- [6] J. H. Kim, M. Park, and I. K. Yu, "Development of real time protective coordination algorithm for HTS power cable," *IEEE Trans. Appl. Supercond.*, vol. 25, no. 3, pp. 3–6, 2015, doi: 10.1109/TASC.2014.2374674.
- [7] SuperPower, "SuperPower 2G HTS wire specifications," 2013. <https://www.superpower-inc.com/specification.aspx>.
- [8] R. Su *et al.*, "Numerical Model of HTS Cable and Its Electric-Thermal Properties," *IEEE Trans. Appl. Supercond.*, vol. 29, no. 5, pp. 0–4, 2019, doi: 10.1109/TASC.2019.2901874.
- [9] W. Xiang *et al.*, "DC Fault Study of a Point-to-Point HVDC System Integrating Offshore Wind Farm using High-Temperature Superconductor DC Cables," *IEEE Trans. Energy Convers.*, vol. 8969, no. c, pp. 1–11, 2021, doi: 10.1109/TEC.2021.3094308.
- [10] T. Jin, J. P. Hong, H. Zheng, K. Tang, and Z. H. Gan, "Measurement of boiling heat transfer coefficient in liquid nitrogen bath by inverse heat conduction method," *J. Zhejiang Univ. Sci. A*, vol. 10, no. 5, pp. 691–696, 2009, doi: 10.1631/jzus.A0820540.
- [11] D. Tzelepis *et al.*, "Impact of synchronous condensers on transmission line protection in scenarios with high penetration of renewable energy sources," *IET Conf. Publ.*, vol. 2020, no. CP771, pp. 1–5, 2020, doi: 10.1049/cp.2020.0095.
- [12] A. O. Rousis, D. Tzelepis, Y. Pipelzadeh, G. Strbac, C. D. Booth, and T. C. Green, "Provision of Voltage Ancillary Services through Enhanced TSO-DSO Interaction and Aggregated Distributed Energy Resources," *IEEE Trans. Sustain. Energy*, vol. 12, no. 2, pp. 897–908, 2021, doi: 10.1109/TSSTE.2020.3024278.